Geophysical Research Letters

RESEARCH LETTER
10.1029/2019GL084988

Constraining the Variability of the Atlantic Meridional Overturning Circulation During the Holocene

Jörg Lippold[1], Frerk Pöppelmeier[1], Finn Süfke[1], Marcus Gutjahr[2], Tyler J. Goepfert[2], Patrick Blaser[1], Oliver Friedrich[1], Jasmin M. Link[3], Lukas Wacker[4], Stefan Rheinberger[1], and Samuel L. Jaccard[5]

[1]Institute of Earth Sciences, Heidelberg University, Heidelberg, Germany, [2]GEOMAR Helmholtz Centre for Ocean Research Kiel, Kiel, Germany, [3]Institute of Environmental Physics, Heidelberg University, Heidelberg, Germany, [4]Institute for Particle Physics, ETH Zürich, Zürich, Switzerland, [5]Institute of Geological Sciences and Oeschger Centre for Climate Change Research, University of Bern, Bern, Switzerland

Key Points:
- High-resolution $^{231}Pa/^{230}Th$ record from the Bermuda Rise for the past 11,000 years presented
- Low variability of Holocene AMOC derived from $^{231}Pa/^{230}Th$, εNd and $\delta^{13}C$
- Duration and magnitude of the 8.2-ka event constrained by sensitivity tests

Supporting Information:
- Supporting Information S1
- Table S1

Correspondence to:
J. Lippold,
joerg.lippold@geow.uni-heidelberg.de

Citation:
Lippold, J., Pöppelmeier, F., Süfke, F., Gutjahr, M., Goepfert, T. J., Blaser, P., et al. (2019). Constraining the variability of the atlantic meridional overturning circulation during the holocene. *Geophysical Research Letters*, *46*, 11,338–11,346. https://doi.org/10.1029/2019GL084988

Received 13 AUG 2019
Accepted 29 SEP 2019
Accepted article online 17 OCT 2019
Published online 29 OCT 2019

Abstract There is a converging body of evidence supporting a measurable slowdown of the Atlantic Meridional Overturning Circulation (AMOC) as climate warms and Northern Hemisphere ice sheets inexorably shrink. Within this context, we assess the variability of the AMOC during the Holocene based on a marine sediment core retrieved from the deep northwest Atlantic, which sensitively recorded large-scale deglacial transitions in deep water circulation. While there is a diffuse notion of Holocene variability in Labrador and Nordic Seas overturning, we report a largely invariable deep water circulation for the last ~11,000 years, even during the meltwater pulse associated with the 8.2-ka event. Sensitivity tests along with high-resolution $^{231}Pa/^{230}Th$ data constrain the duration and the magnitude of possible Holocene AMOC variations. The generally constant baseline during the Holocene suggests attenuated natural variability of the large-scale AMOC on submillennial timescales and calls for compensating effects involving the upstream components of North Atlantic Deep Water.

1. Introduction

Atlantic Meridional Overturning Circulation (AMOC) variability has been linked to changes in the formation rate of North Atlantic Deep Water (NADW). Recent studies suggest a steady decline of the AMOC strength during the past decades and centuries (Caesar et al., 2018; Rahmstorf et al., 2015; Thornalley et al., 2018) raising concerns about its vulnerability in the face of global warming and accelerating Greenland ice sheet melting. Painstaking efforts have been devoted to reconstruct changes in AMOC dynamics in the recent geological past in order to better predict its future evolution. These investigations provide ample evidence for large-scale glacial and deglacial AMOC reorganizations as inferred from independent proxy approaches (Howe, Piotrowski, Noble, et al., 2016; Lippold et al., 2016; Lynch-Stieglitz, 2017; Marchitto & Broecker, 2006; McManus et al., 1999; Oppo et al., 2018; Praetorius et al., 2008; Roberts et al., 2010). While there is a general sense that AMOC variability was subdued during the Holocene compared with the last glacial termination (Keigwin & Boyle, 2000; Oppo et al., 2003), proxy evidence is often contradictory. Discrepancies remain regarding the timing, overall tendency, and amplitude of deep water export variations based on a wealth of various proxy records, mainly focusing on upstream tributaries of NADW including the Labrador Sea Water (LSW) and Nordic Seas Overflow Waters (Ellison et al., 2006; Hall et al., 2004; Hoogakker et al., 2011; Keigwin et al., 2005; Kissel et al., 2013; Kleiven et al., 2008; Mjell et al., 2015; Moffa-Sánchez & Hall, 2017; Thornalley et al., 2013).

Here we aim at reconstructing large-scale AMOC variability for the Holocene, combining high-resolution $^{231}Pa/^{230}Th$, εNd, and $\delta^{13}C$ records with existing data from Bermuda Rise sediments, which sensitively recorded past changes in AMOC dynamics (Böhm et al., 2015; Deaney et al., 2017; Gutjahr & Lippold, 2011; Henry et al., 2016; Keigwin & Boyle, 2000; McManus et al., 2004; Rempfer et al., 2017; Roberts et al., 2010). Existing Holocene data sets from this area are not available in sufficient temporal resolution or have been obtained from potentially less sensitive locations, hindering identification of short-scale AMOC oscillations (Hoffmann et al., 2018; Lippold et al., 2016; McManus et al., 2004; Ng et al., 2018; Rempfer et al., 2017).

Seawater-derived Nd isotope signatures recorded in marine sediments (εNd) allow distinguishing the major water masses bathing the Atlantic basin. NADW is characterized by distinctively less radiogenic (i.e., lower)

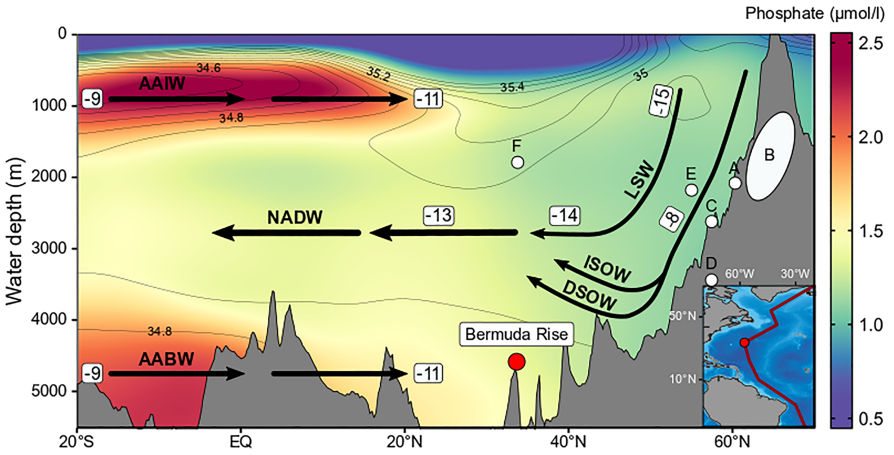

Figure 1. Schematic view of water masses in the NW Atlantic. Distinct water masses (black arrows schematically indicate the flow direction) such as Antarctic Bottom Water (AABW), Antarctic Intermediate Water (AAIW), or the constituents of NADW (mainly Denmark Strait Overflow Water [DSOW], Iceland-Scotland Overflow Water [ISOW], and Labrador Sea Water [LSW]) are distinguishable by phosphate concentrations (colors; Garcia et al., 2014), salinity (contour lines) and by εNd (numbers in white boxes, (Lambelet et al., 2016)). The map inlay gives the position of the Bermuda Rise with the north-south transect of the shown phosphate concentrations. White circles with letters indicate locations from other Holocene data shown in Figure 3. A: GS06-144 08GC (Mjell et al., 2015), B: Iceland slope stack (Thornalley et al., 2013), C: MD99-2251 (Ellison et al., 2006), D: MD03-2665 (Kleiven et al., 2008), E: Ocean Drilling Program Site 980 (Oppo et al., 2003), F: KN140-2-51GGC (Hoffmann et al., 2018).

εNd signatures (mostly due to the contribution of very unradiogenic LSW (εNd ~ −15) compared to more radiogenic signatures of Southern Component Water (εNd ~ −9, Figure 1; e.g., (Lambelet et al., 2016; Stichel et al., 2015). Similarly, the stable carbon isotope composition ($\delta^{13}C$) of seawater recorded by epibenthic foraminifera, indicative of the accumulation of remineralized carbon in the ocean interior, represents a debated (Gebbie et al., 2015; Howe, Piotrowski, Noble, et al., 2016; Schmittner et al., 2013; Voigt et al., 2017), yet long-standing proxy for reconstructions of water mass distribution (Curry & Oppo, 2005; Keigwin, 2004; Oppo et al., 2003). Both tracers thus provide largely independent and complementary evidence reflecting past changes in the relative contributions of water masses originating from the North Atlantic and the Southern Ocean. In contrast, sedimentary $^{231}Pa/^{230}Th$ reflects kinematic changes in ocean circulation and provides a quantitative measure of the integrated AMOC strength (Deng et al., 2018; Yu et al., 1996). A difference in the removal timescale between both radioisotopes causes a deficit of ^{231}Pa relative to ^{230}Th in marine sediments in the Atlantic Ocean, the extent of which is related to the strength of meridional export of NADW (Luo et al., 2010; Marchal et al., 2000; Rempfer et al., 2017). Hence, low $^{231}Pa/^{230}Th$ values, below the production ratio of 0.093, reflect strong NADW advection, while higher values are consistent with a weaker AMOC state.

2. Materials and Methods

Ocean Drilling Program (ODP) Site 1063 (33°41.2′N, 57°36.9′W) was recovered from the Bermuda Rise during ODP Leg 172 from a water depth of 4,584 m (Keigwin et al., 1998). Numerous investigations targeting past changes in ocean circulation patterns have been performed based on marine archives from the Bermuda Rise (see overview on core locations and studies in the supporting information S1; Böhm et al., 2015; Deaney et al., 2017; Gutjahr & Lippold, 2011; Henry et al., 2016; Keigwin & Boyle, 2008; Keigwin & Boyle, 2000; Lippold et al., 2009; McManus et al., 2004; Roberts et al., 2010). From the Holocene section of ODP Site 1063 Hole A and D (0–110 cm) 81 samples for $^{231}Pa/^{230}Th$ (71 for εNd and 17 for $\delta^{13}C$) have been taken allowing for high-resolution kinematic reconstructions of past changes in AMOC dynamics.

2.1. Age Model

The Holocene age model for ODP Site 1063 is based on 13 new radiocarbon age control points covering the past 11,000 years. The ^{14}C dates were generated by Accelerator Mass Spectrometry at ETH Zurich (Wacker

et al., 2013) on at least 300-μg *Globigerinoides ruber* (white and pink variety; supporting information S2). Age uncertainties are given as 1 sigma standard deviations. The calibration of the radiocarbon ages was performed with Calib7.10 using the MARINE13 (Reimer et al., 2013) data set and assuming a constant 400-year surface radiocarbon reservoir age. One additional age control point is given by the minimum in magnetic susceptibility during the Younger Dryas (Roberts et al., 2010). The age model of Hole A is based on the three ^{14}C dates back to 2.5 ka. The part of Hole A older than 2.5 ka has been aligned to the ^{14}C-constrained age model of Hole D by aligning the magnetic susceptibility signals of both holes (supporting information S2).

2.2. Neodymium Isotope Analyses

The $^{143}Nd/^{144}Nd$ ratio (expressed in εNd units, i.e., the deviation of the measured $^{143}Nd/^{144}Nd$ from that of the Chondritic Uniform Reservoir in parts per 10,000) is used as a quasi-conservative tracer to reconstruct changes in the source and mixing of water masses (Frank, 2002; Piotrowski et al., 2005). The water Nd isotope signal was extracted from bulk sediments of ODP Site 1063 following the leaching and measurement procedures described by Blaser et al. (2019). Nd isotope measurements were carried out with a Thermo Fisher Neptune Plus inductively coupled plasma mass spectrometer at GEOMAR Kiel. Raw ratios were corrected for isobaric interference of ^{144}Sm and for mass bias by an exponential law calibrating to a stable ratio of $^{146}Nd/^{144}Nd = 0.7219$. Corrected $^{143}Nd/^{144}Nd$ were then normalized to bracketing standards of JNdi-1 with a value of 0.512115 (Tanaka et al., 2000). The shown uncertainties are the double standard deviation of in-house standard solutions measured repeatedly throughout the same sessions and lie between 0.07 and 0.37 epsilon units.

2.3. Uranium, Thorium, and Protactinium Isotope Analyses

For $^{231}Pa/^{230}Th$ analyses bulk concentrations of ^{231}Pa, ^{230}Th, ^{232}Th, and ^{238}U have been measured. Per sample approximately 0.1 g of bulk sediment was weighed and then spiked with ^{233}Pa, ^{229}Th, and ^{236}U followed by total digestion in a mixture of concentrated HCl, HNO_3, and HF. Pa, Th, and U were separated by anion exchange column chromatography (Süfke et al., 2018). The ^{233}Pa-spike was calibrated against the reference standard material UREM-11 and an internal pitchblende standard (Fietzke et al., 1999). Following standard ICP-MS methods (Böhm et al., 2015; Lippold et al., 2009), measurements of protactinium were performed on a Thermo Finnigan ELEMENT2 at Heidelberg University, while uranium and thorium were measured on a Thermo Fisher Neptune Plus MC-ICP-MS at GEOMAR Kiel. Full process blank contributions to ^{230}Th, ^{232}Th, and ^{238}U were lower than 1%, for ^{231}Pa below 1.5% and thus negligible. Average uncertainties for each isotopic concentrations are 3.2% (^{231}Pa), 1.5% (^{230}Th), 1.1% (^{232}Th), and 0.8% (^{238}U).

Total ^{231}Pa and ^{230}Th activities were corrected for detrital and authigenic input (Henderson & Anderson, 2003) using a lithogenic activity ratio of $^{238}U/^{232}Th = 0.47$ based on the continuously low values of this ratio obtained from a 300-ka record of this core (Christl et al., 2010) also following the suggestions by Bourne et al. (2012). Given the relatively young ages of the sediment samples, the authigenic contribution is marginal. Similarly, due to the proportion of the excess fractions the resulting $^{231}Pa/^{230}Th$ is insensitive to the choice of the lithogenic $^{238}U/^{232}Th$ background (e.g., average increase of 0.7% in $^{231}Pa/^{230}Th$ for $^{238}U/^{232}Th = 0.6$ instead of 0.47).

2.4. Stable Carbon Isotope Analyses

For stable carbon isotope analyses, dried and weighed sediment samples were disaggregated in distilled water and washed over a 63-μm mesh. Samples were subsequently dry-sieved into two fractions: 63 to 150 and >150 μm. One to five specimens of the benthic foraminifera *Cibicidoides wuellerstorfi* were picked from the >150-μm dried sediment fraction. The carbon-isotope composition of *C. wuellerstorfi* was analyzed using a Thermo Finnigan MAT253plus gas source mass spectrometer coupled to a Kiel IV carbonate preparation device at the Institute of Earth Sciences, Heidelberg University. Values are reported relative to Vienna Pee Dee Belemnite through the analysis of an in-house standard calibrated to IAEA-603. The precision for standards run parallel to the analyzed samples is better than 0.03‰ (at 1σ level).

2.5. Measurements of Biogenic Opal

To assess the potential influence of changes in particulate biogenic opal fluxes on $^{231}Pa/^{230}Th$, its preserved concentration in the sediment was measured. The measurements followed the automated procedure for analysis of dissolved silica applying molybdate-blue spectrophotometry (Müller & Schneider, 1993) and were

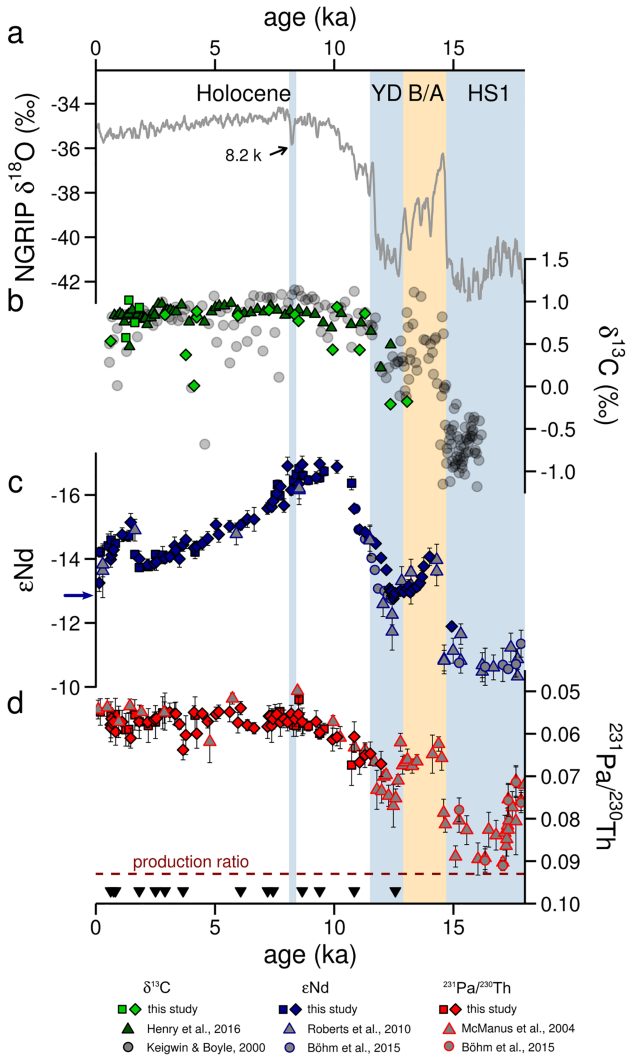

Figure 2. Bermuda Rise Holocene Atlantic Meridional Overturning Circulation records. (a) Oxygen isotope record of the NGRIP ice core (Andersen et al., 2004). (b) Benthic foraminiferal $\delta^{13}C$ data from the Bermuda Rise (Henry et al., 2016; Keigwin & Boyle, 2000; this study). (c) Bermuda Rise bottom water εNd (Böhm et al., 2015; Roberts et al., 2010; this study). The blue arrow indicates modern NW Atlantic εNd (Lambelet et al., 2016). (d) Bermuda Rise $^{231}Pa/^{230}Th$ (Böhm et al., 2015; McManus et al., 2004; this study). The dashed line indicates the production ratio of both radioisotopes in seawater. Black triangles indicate ^{14}C-based age control points. Colored vertical bars highlight the time periods of Heinrich Stadial 1 (HS1), Bølling/Allerød (B/A), Younger Dryas (YD), and the 8.2-ka event. Diamonds represent data obtained from Hole D, squares from Hole A of Ocean Drilling Program Site 1063.

performed at GEOMAR, Kiel. Bulk concentrations ranged from 0.9% to 2.2% with an error based on repeated measurements of replicates in the range of 2–40% (2 RSD).

3. Results

The new epibenthic foraminiferal $\delta^{13}C$ generally cluster around high values, ranging between 0.5 and 1.0 corroborating available data (Henry et al., 2016; Keigwin & Boyle, 2000) indicative of little variation in water mass sourcing and/or air-sea gas exchange and remineralization during the Holocene (Figure 2). In contrast, our new high-resolution Nd isotope record reveals a pronounced trend of decreasing εNd values in the aftermath of the YD with values as unradiogenic as −17 at the onset of the Holocene. This is followed by a gradual recovery toward more radiogenic values trending to modern seawater values (Figure 2c, ref. (Lambelet et al., 2016)). This unexpected early Holocene variability in Nd isotope signature could potentially contradict the relatively constant $\delta^{13}C$ if interpreted at face value in terms of conservative water mass mixing. In turn, $^{231}Pa/^{230}Th$ with constant and low values residing clearly and consistently below the production ratio mirrors the $\delta^{13}C$ trend. The new high-resolution data are consistent with the existing, lower-resolution Bermuda Rise $^{231}Pa/^{230}Th$ record (McManus et al., 2004) exhibiting low variability (max: 0.065, min: 0.052, average: 0.057 for the last 10 ka). We obtained the highest resolution of the record around 8 ka bracketing the prominent 8.2-ka event (Thomas et al., 2007), yet without recording any significant variation around this time period.

4. Discussion

The high-resolution epibenthic foraminifera $\delta^{13}C$ records (Figure 2; Henry et al., 2016; Keigwin & Boyle, 2000; this study) highlight the persistent presence of NADW at the Bermuda Rise during the Holocene. These observations are further supported by consistently unradiogenic bottom water εNd signatures (εNd between −17 and −13) throughout the last ~12 ka. However, the εNd record arguably shows more structure when compared to the $\delta^{13}C$ record, notably featuring a pronounced negative early Holocene excursion. Such a postdeglacial unradiogenic εNd pulse is unlikely to reflect changes in water mass distribution alone (Pöppelmeier et al., 2018), and it has been hypothesized that this excursion has been caused, in part, by poorly weathered lithogenic material supplied to the Labrador Sea seabed as ice sheets retreated in the aftermath of the deglaciation (Howe, Piotrowski, & Rennie, 2016). The expression of the unradiogenic peak in the early Holocene attenuates southward, supporting the hypothesis of a signal originating predominantly from the Labrador Sea with material transported downslope and along the continental margin by nepheloid layers (Pöppelmeier et al., 2019). A larger data set in particular from the Labrador Sea would be required to better quantify these processes creating such a transient, unradiogenic excursion. However, due to its unquestionably unradiogenic character (εNd consistently below −13) combined with constantly high $\delta^{13}C$ values, it seems inescapable that NADW continuously bathed the deep NW Atlantic over the course of the Holocene.

Furthermore, sedimentary $^{231}Pa/^{230}Th$ data measured on the same samples provide means to quantify the meridional advection of NADW. Compared to the large deglacial $^{231}Pa/^{230}Th$ excursions related to prominent AMOC oscillations (McManus et al., 2004), the Holocene values remain constantly low (Figure 2d),

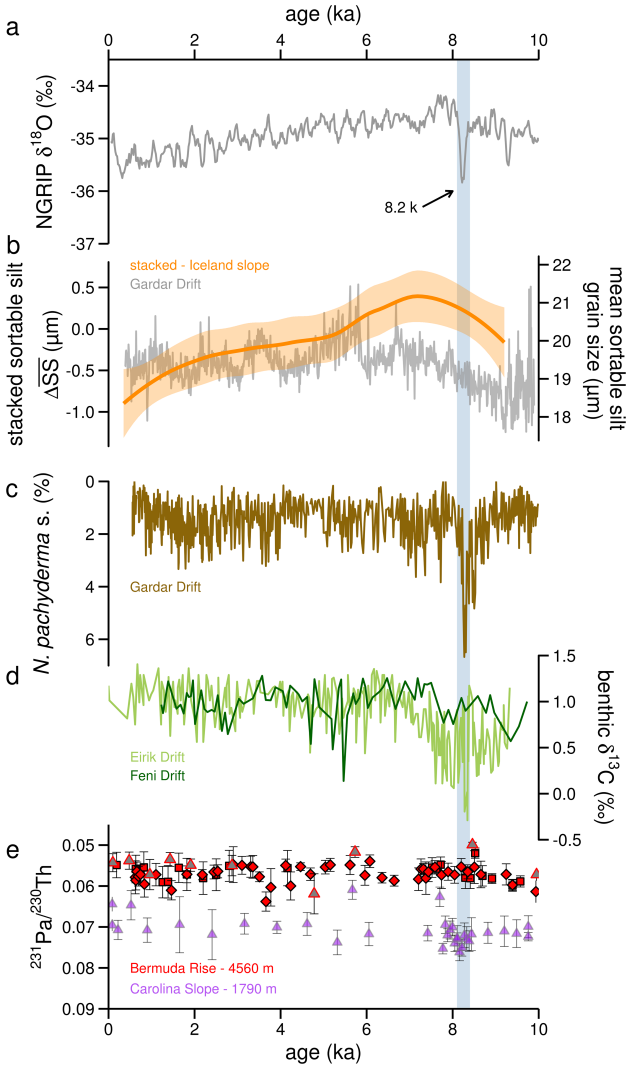

Figure 3. Expanded view on $^{231}Pa/^{230}Th$ in comparison to NGRIP and hydrographic proxies from a variety of North Atlantic studies indicating different trends. The blue bar indicates the time period of the 8.2-ka event as manifested in the NGRIP record. (a) Oxygen isotope record of the NGRIP ice core (Andersen et al., 2004). (b) Sortable silt records of ISOW strength from (right axis) Core GS06-144 08GC (Mjell et al., 2015) and an (left axis) Iceland slope stack (Thornalley et al., 2013). (c) Relative abundance of the polar foraminifer *N. pachyderma* from the Core MD99-2251 (Ellison et al., 2006). (d) $\delta^{13}C$ of *C. wuellerstorfi* from (bright) Core MD03-2665 (Kleiven et al., 2008) and from (dark) ODP Site 980 (Oppo et al., 2003). (e) High-resolution Holocene $^{231}Pa/^{230}Th$ from the ODP Site 1063 (red, this study and McManus et al., 2004) and from the shallower core KN140-2-51GGC (purple) (Hoffmann et al., 2018).

indicative of a stable and vigorous NADW overturning cell. While there is debate as to which degree varying opal fluxes may influence downcore $^{231}Pa/^{230}Th$ records (Ng et al., 2018), the preserved opal concentrations in Holocene sediments of ODP Site 1063 remain consistently low during the Holocene (<2.5%) rendering a perceptible influence on the very stable $^{231}Pa/^{230}Th$ pattern unlikely. Both low opal concentrations and constant $^{231}Pa/^{230}Th$ values throughout the Holocene have been also reported recently from a shallower site (KN140-2-51GGC, 32.783°N, 76.283°W, 1,790-m water depth) closer to the margin (Figure 3f; Hoffmann et al., 2018). Similarly, other potential particle-induced effects on $^{231}Pa/^{230}Th$ like bottom or boundary scavenging (Hayes, Anderson, Fleisher, Huang, et al., 2015; Hayes, Anderson, Fleisher, Vivancos, et al., 2015; Rempfer et al., 2017) must have been constant and of secondary order, as witnessed by the virtually invariable $^{231}Pa/^{230}Th$ records from both locations over the course of the Holocene (comparisons of particle fluxes with $^{231}Pa/^{230}Th$ are shown in Figure S3). While the higher sedimentation rates of 51GGC would allow higher temporal resolution, its $^{231}Pa/^{230}Th$ record is potentially less sensitive to AMOC variations due to its shallower and more southern location (Rempfer et al., 2017). In contrast to these observations, previous studies did report variations in the intensities of Overflow Waters and/or LSW overturning rates (e.g., Ayache et al., 2018; Hall et al., 2004; Hoogakker et al., 2011; Kissel et al., 2013; Kleiven et al., 2008; Mjell et al., 2015; Moffa-Sánchez & Hall, 2017; Thornalley et al., 2013; Figure 3) but did not yield a coherent picture regarding the timing and amplitude of these variations. Within the perspective of our data, these observed variations appear to remain spatially limited to the tributaries of NADW possibly compensating for each other and thus not affecting the integrated downstream NADW circulation scheme (Moffa-Sanchez et al., 2015; Renssen et al., 2005).

Importantly, we found neither a gradual temporal AMOC trend (as implied by the steady decrease of Greenland's $\delta^{18}O$-based temperature record (Figure 3a) or observed for Iceland-Scotland Overflow Water (e.g., Thornalley et al., 2013, Figure 3b) nor an abrupt decline associated with the 8.2-ka cooling. This is somewhat surprising since the effects of meltwater outbursts and/or ice-saddle collapse that have been proposed to account for the prominent 8.2-ka event (Hoffman et al., 2012; Matero et al., 2017) are expected to be capable of substantially weakening the AMOC and have been recorded in high-resolution paleoceanographic reconstructions (Ellison et al., 2006; Hall et al., 2004; Kleiven et al., 2008; Praetorius et al., 2008). Thus, the absence of any discernible $^{231}Pa/^{230}Th$ excursion centered around 8.2 ka raises questions related to the temporal resolution capacity of $^{231}Pa/^{230}Th$ in sedimentary records. There is only limited knowledge on the exact duration of the 8.2-ka event meltwater outburst (most probably in the range of <200 years; Cheng et al., 2009) and no clear agreement on the freshwater source and routing (Carlson & Clark, 2012; Hoogakker et al., 2011; Kissel et al., 2013; Kleiven et al., 2008; Mjell et al., 2015; Oppo et al., 2003). In order to assess the magnitude and duration of a potential AMOC perturbation associated with the 8.2-ka event, we apply a conceptual box model (Christl, 2007; supporting information S4) simulating the $^{231}Pa/^{230}Th$ signal recorded in the sediment. Variations in sedimentary $^{231}Pa/^{230}Th$ ratios are in the first-order functions of (i) the oceanic residence time of ^{231}Pa, (ii) sediment accumulation, (iii) bioturbation, and (iv) the magnitude and duration of the perturbation affecting the meridional advection of ^{231}Pa. Using the prominent AMOC perturbations characterizing the Younger Dryas (YD) and Heinrich Stadial 1 (HS1) as test cases, our model faithfully reproduces the

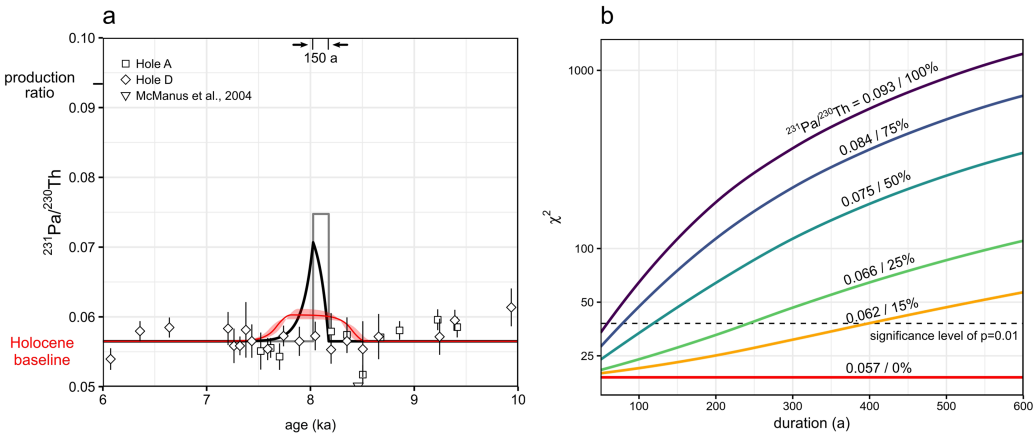

Figure 4. Bermuda Rise $^{231}Pa/^{230}Th$ compared to expected signal strength. (a) $^{231}Pa/^{230}Th$ around the 8.2-ka event (open symbols) and modeled increase of $^{231}Pa/^{230}Th$ from the Holocene baseline represented by the gray rectangular wave signal, which is smoothed by the oceanic residence time of ^{231}Pa (black, see supporting information S4 for model description). The red curve (including an uncertainty range of 20% accounting for the maximum error on the sedimentation rate) delineates the resulting sediment signal blurred by bioturbation As an example the scenarios of a hypothetical Atlantic Meridional Overturning Circulation reduction by 50% for 150 years is shown, which is expected to be still distinguishable from the observations. Further scenario outputs with varying parameter sets are demonstrated in supporting information S6. (b) Goodness of fit measured as χ^2 between model and data for different event durations. Line colors indicate $^{231}Pa/^{230}Th$ levels corresponding to Atlantic Meridional Overturning Circulation reductions. Dashed line shows the significance level equivalent to a p value of 0.01 calculated from the χ^2 distribution for $d = n - 1 = 20$ degrees of freedom ($n = 21$; data points in the relevant time interval of 7–9 ka). Scenarios above the dashed line are considered to be inconsistent with the observed constant $^{231}Pa/^{230}Th$, while scenarios below cannot be rejected.

amplitude of both associated $^{231}Pa/^{230}Th$ peaks (McManus et al., 2004) at the Bermuda Rise (supporting information S5). In comparison to the YD and HS1 the sedimentation rates at ODP Site 1063 were lower during the 8.2-ka event (~8.3 cm/ka). Hence, bioturbation is expected to attenuate the sedimentary response (Figure 4a, red) of a changing oceanic $^{231}Pa/^{230}Th$ signal (Figure 4a, black). In a next step we compare the high-resolution $^{231}Pa/^{230}Th$ data (31 data points between 7 and 10 ka) to the model outputs of systematically varied parameters (i.e., event duration, event magnitude, and bioturbation length; supporting information S6). The multitude of parameters produces hypothetical $^{231}Pa/^{230}Th$ profiles, which mostly significantly differ from our observations, constraining magnitude and in particular the duration of a hypothetical AMOC decrease (supporting information S6). For example, the model outputs suggest that an AMOC perturbation resulting in an ~50% $^{231}Pa/^{230}Th$ increase, associated with a 150 years lasting 8.2-ka event, should still be distinguishable from the average Holocene $^{231}Pa/^{230}Th$ values (0.057; Figure 4a). For a bioturbation length of 6 cm (global mean; Teal et al., 2008) we assess the degree of convergence between modeled and observational data by means of the goodness of fit measured as χ^2 applying a level of significance of $p = 0.01$ (Figure 4b). We find that if the reduction in AMOC lasted for longer than ~125 years, it could not have been excessively severe (a HS1-like perturbation would have been observable for event durations of ~75 years or more, Figure 4b, blue), while $^{231}Pa/^{230}Th$ increases to YD-levels of around 0.075 (e.g., Figure 4a) are expected to be recognizable in the record after ~125 years (Figure 4b, dark green). Less pronounced reductions, however, are beyond the resolution capacity of the record and are not statistically different from the null hypothesis ($^{231}Pa/^{230}Th = 0.057$, red) if not lasting at least >250 years (Figure 4b, bright green).

5. Conclusion

We present new $^{231}Pa/^{230}Th$ data (supported by εNd and $\delta^{13}C$) from the Bermuda Rise complementing the existing records of the last glacial cycle in high resolution for the Holocene. While εNd and $\delta^{13}C$ data document the continuous presence of NADW in the deep NW Atlantic (with εNd showing an unradiogenic excursion due to variable input from the Labrador Sea (Howe, Piotrowski, & Rennie, 2016; Pöppelmeier et al., 2018; Pöppelmeier et al., 2019) $^{231}Pa/^{230}Th$ indicates a constant export of ^{231}Pa by NADW throughout the Holocene without any perceivable interruptions on millennial scale. Since variations in the strength of NADW forming components further upstream have been observed, these water masses may have

compensated for each other resulting in a stable NADW circulation on basin scale (Moffa-Sanchez et al., 2015; Renssen et al., 2005). While a strong large-scale AMOC persisted during the Holocene, smaller-scale and/or shorter perturbations may have been unrecorded by the $^{231}Pa/^{230}Th$ proxy. Based on sensitivity tests compared to observations, we constrain a hypothetical AMOC reduction around the 8.2-ka event as a function of its magnitude and duration (Figure 4b). We found that the constant $^{231}Pa/^{230}Th$ observed between 9 and 7 ka do not allow YD-like AMOC perturbations longer than 125 years. But smaller perturbations (e.g., <25%) could have been persisted for ~200 years, before it would be recognizable from our record. Such a limited AMOC reduction below ~25% for no longer than 200 years across the 8.2-ka event would be in agreement with scenarios of a confined impact on the AMOC (Born & Levermann, 2010; Condron & Winsor, 2011; Morrill et al., 2013) as well as with previous $^{231}Pa/^{230}Th$ data (Hoffmann et al., 2018) from a shallower core location of higher sedimentation rate. Considering the modern ~15% decline in the Deep Western Boundary Current strength (Caesar et al., 2018; Thornalley et al., 2018), our results imply that such a reduction could have already occurred during the Holocene but must have been of limited duration since it was not captured by $^{231}Pa/^{230}Th$.

Acknowledgments
This research used sediment samples provided by the Ocean Discovery Program (ODP), which is supported by NSF and participating countries under management of Joint Oceanographic Institutions (JOI) Inc. Analytical support and provision of infrastructure from M. Brückner and M. Regelous is acknowledged. We thank M. Deininger, J. McManus, D. Thornalley, and the OC3/iPODS workshop participants in Cambridge (UK) 2018 for valuable discussions. Data presented in this study are available in the supporting information and on the PANGAEA website https://doi.pangaea.de/10.1594/PANGAEA.907381. Financial support for this research was provided by the Emmy-Noether Programme of the Deutsche Forschungsgemeinschaft (DFG) through Grant Li1815/4 and the Swiss National Science Foundation (SNSF Grant 200021_163003 to S. L. J.).

References

Andersen, K. K., Azuma, N., Barnola, J. M., Bigler, M., Biscaye, P., Caillon, N., et al., & North Greenland Ice Core Project members (2004). North Greenland Ice Core Project, High-resolution record of Northern Hemisphere climate extending into the last interglacial period. *Nature*, *431*(7005), 147–151. https://doi.org/10.1038/nature02805

Ayache, M., Swingedouw, D., Mary, Y., Eynaud, F., & Colin, C. (2018). Multi-centennial variability of the AMOC over the Holocene: A new reconstruction based on multiple proxy-derived SST records. *Global and Planetary Change*, *170*, 172–189. https://doi.org/10.1016/j.gloplacha.2018.08.016

Blaser, P., Pöppelmeier, F., Schulz, H., Gutjahr, M., Frank, M., Lippold, J., Heinrich, H., et al. (2019). The resilience and sensitivity of Northeast Atlantic deep water εNd to overprinting by detrital fluxes over the past 30,000 years. *Geochimica et Cosmochimica Acta*, *245*, 79–97. https://doi.org/10.1016/j.gca.2018.10.018

Bourne, M., Thomas, A., Niocaill, C., & Henderson, G. (2012). Improved determination of marine sedimentation rates using 230Thxs. *Geochemistry Geophysics Geosystems*, *13*(1), Q09017.

Böhm, E., Lippold, J., Gutjahr, M., Frank, M., Blaser, P., Antz, B., et al. (2015). Strong and deep Atlantic Meridional Overturning Circulation during the last glacial cycle. *Nature*, *517*(7532), 73–76. https://doi.org/10.1038/nature14059

Born, A., & Levermann, A. (2010). The 8.2 ka event: Abrupt transition of the subpolar gyre toward a modern North Atlantic circulation. *Geochemistry, Geophysics, Geosystems*, *11*, Q06011. https://doi.org/10.1029/2009GC003024

Caesar, L., Rahmstorf, S., Robinson, A., Feulner, G., & Saba, V. (2018). Observed fingerprint of a weakening Atlantic Ocean overturning circulation. *Nature*, *556*(7700), 191–196. https://doi.org/10.1038/s41586-018-0006-5

Carlson, A., & Clark, P. (2012). Ice sheet sources of sea level rise and freshwater discharge during the last deglaciation. *Reviews of Geophysics*, *50*, RG4007. https://doi.org/10.1029/2011RG000371

Cheng, H., Fleitmann, D., Edwards, R. L., Wang, X., Cruz, F. W., Auler, A. S., et al. (2009). Timing and structure of the 8.2 kyr B.P. event inferred from δ18O records of stalagmites from China, Oman, and Brazil. *Geology*, *37*(11), 1007–1010. https://doi.org/10.1130/G30126A.1

Christl, M. (2007). Sensitivity and response of beryllium-10 in marine sediments to rapid production changes (geomagnetic events): A box model study. *Geochemistry, Geophysics, Geosystems*, *8*, Q09015. https://doi.org/10.1029/2007GC001598

Christl, M., Lippold, J., Steinhilber, F., Bernsdorff, F., & Mangini, A. (2010). Reconstruction of global ^{10}Be production over the past 250 ka from highly accumulating Atlantic drift sediments. *Quaternary Science Reviews*, *29*(19-20), 2663–2672. https://doi.org/10.1016/j.quascirev.2010.06.017

Condron, A., & Winsor, P. (2011). A subtropical fate awaited freshwater discharged from glacial Lake Agassiz. *Geophysical Research Letters*, *38*, L03705. https://doi.org/10.1029/2010GL046011

Curry, W., & Oppo, D. (2005). Glacial water mass geometry and the distribution of $d^{13}C$ of CO_2 in the western Atlantic Ocean. *Paleoceanography*, *20*, PA1017. https://doi.org/10.1029/2004PA001021

Deaney, E. L., Barker, S., & van de Flierdt, T. (2017). Timing and nature of AMOC recovery across Termination 2 and magnitude of deglacial CO_2 change. *Nature Communications*, *8*(1), 14595. https://doi.org/10.1038/ncomms14595

Deng, F., Henderson, G. M., Castrillejo, M., & Perez, F. F. (2018). Evolution of ^{231}Pa and ^{230}Th in overflow waters of the North Atlantic. *Biogeosciences*, *15*(23), 7299–7313. https://doi.org/10.5194/bg-15-7299-2018

Ellison, C., Chapman, M., & Hall, I. (2006). Surface and deep ocean interactions during the cold climate event 8200 years ago. *Science*, *312*(5782), 1929–1932. https://doi.org/10.1126/science.1127213

Fietzke, J., Bollhöfer, A., Frank, N., & Mangini, A. (1999). Pa determination in manganese crust VA12/2 by TIMS. *Nuclear Instruments and Methods in Physics Research B*, *149*(3), 353–360. https://doi.org/10.1016/S0168-583X(98)00912-4

Frank, M. (2002). Radiogenic isotopes: Tracers of past ocean circulation and erosional input. *Reviews of Geophysics*, *40*(1), 1001. https://doi.org/10.1029/2000RG000094

Garcia, H. E., Locarnini, R. A., Boyer, T. P., Antonov, J. I., Baranova, O. K., Zweng, M. M., et al. (2014). World Ocean Atlas 2013, Volume 4: Dissolved Inorganic Nutrients (phosphate, nitrate, silicate). In S. Levitus & A. Mishonov Technical Ed.; NOAA Atlas NESDIS 76 (25 pp.)

Gebbie, G., Peterson, C. D., Lisiecki, L. E., & Spero, H. J. (2015). Global-mean marine $\delta^{13}C$ and its uncertainty in a glacial state estimate. *Quaternary Science Reviews*, *125*, 144–159. https://doi.org/10.1016/j.quascirev.2015.08.010

Gutjahr, M., & Lippold, J. (2011). Early arrival of southern source water in the deep North Atlantic prior to Heinrich event 2. *Paleoceanography*, *26*, PA2101. https://doi.org/10.1029/2011PA002114

Hall, I., Bianchi, G. G., & Evans, J. R. (2004). Centennial to millennial scale Holocene climate-deep water linkage in the North Atlantic. *Quaternary Science Reviews*, *23*(14-15), 1529–1536. https://doi.org/10.1016/j.quascirev.2004.04.004

Hayes, C., Anderson, R. F., Fleisher, M. Q., Huang, K.-F., Robinson, L. F., Lu, Y., et al. (2015). ^{230}Th and ^{231}Pa on GEOTRACES GA03, the U.S. GEOTRACES North Atlantic transect, and implications for modern and paleoceanographic chemical fluxes. *Deep Sea Research Part II: Topical Studies in Oceanography*, *116*, 29–41. https://doi.org/10.1016/j.dsr2.2014.07.007

Hayes, C., Anderson, R. F., Fleisher, M. Q., Vivancos, S. M., Lam, P. J., Ohnemus, D. C., et al. (2015). Intensity of Th and Pa scavenging partitioned by particle chemistry in the North Atlantic Ocean. *Marine Chemistry*, *170*, 49–60. https://doi.org/10.1016/j.marchem.2015.01.006

Henderson, G., & Anderson, R. (2003). The U-series toolbox for paleoceanography, Uranium Series Geochemistry. *Reviews in Mineralogy and Geochemistry*, *128*(52), 493–531.

Henry, L. G., McManus, J. F., Curry, W. B., Roberts, N. L., Piotrowski, A. M., & Keigwin, L. D. (2016). North Atlantic ocean circulation and abrupt climate change during the last glaciation. *Science*, *353*(6298), 470–474. https://doi.org/10.1126/science.aaf5529

Hoffman, J. S., Carlson, A. E., Winsor, K., Klinkhammer, G. P., LeGrande, A. N., Andrews, J. T., & Strasser, J. C. (2012). Linking the 8.2 ka event and its freshwater forcing in the Labrador Sea. *Geophysical Research Letters*, *39*, L18703. https://doi.org/10.1029/2012GL053047

Hoffmann, S. S., McManus, J. F., & Swank, E. (2018). Evidence for stable Holocene basin-scale overturning circulation despite variable currents along the Deep Western Boundary of the North Atlantic Ocean. *Geophysical Research Letters*, *45*(24), 13,427–13,436. https://doi.org/10.1029/2018GL080187

Hoogakker, B. A. A., Chapman, M. R., McCave, I. N., Hillaire-Marcel, C., Ellison, C. R. W., Hall, I. R., & Telford, R. J. (2011). Dynamics of North Atlantic Deep Water masses during the Holocene. *Paleoceanography*, *26*, PA4214. https://doi.org/10.1029/2011PA002155

Howe, J., Piotrowski, A. M., Noble, T. L., Mulitza, S., Chiessi, C. M., & Bayon, G. (2016). North Atlantic Deep Water Production during the Last Glacial Maximum. *Nature Communications*, *7*, 11765. https://doi.org/10.1038/ncomms11765

Howe, J. N. W., Piotrowski, A. M., & Rennie, V. C. F. (2016). Abyssal origin for the early Holocene pulse of unradiogenic neodymium isotopes in Atlantic seawater. *Geology*, *44*(10), 831–834. https://doi.org/10.1130/G38155.1

Keigwin, D., & Boyle, E. (2008). Did North Atlantic overturning halt 17,000 years ago? *Paleoceanography*, *23*, PA1101. https://doi.org/10.1029/2007PA001500

Keigwin, L. (2004). Radiocarbon and stable isotope constraints on Last Glacial Maximum and Younger Dryas ventilation in the western North Atlantic. *Paleoceanography*, *19*, PA4012. https://doi.org/10.1029/2004PA001029

Keigwin, L., & Boyle, E. (2000). Detecting Holocene changes in thermohaline circulation. *PNAS*, *97*(4), 1343–1346. https://doi.org/10.1073/pnas.97.4.1343

Keigwin, L., Rio, D., Acton, G., et al. (1998). Bermuda Rise and Sohm abyssal plain, Sites 1063 and 1064. In *Proceedings of the Ocean Drilling Program, Initial Reports*, (Vol. 172, chap. 6, 251). College Station, TX: Ocean Drilling Program.

Keigwin, L. D., Sachs, J. P., Rosenthal, Y., & Boyle, E. A. (2005). The 8200 year B.P. event in the slope water system, western subpolar North Atlantic. *Paleoceanography*, *20*, PA2003. https://doi.org/10.1029/2004PA001074

Kissel, C., Van Toer, A., Laj, C., Cortijo, E., & Michel, E. (2013). Variations in the strength of the North Atlantic bottom water during Holocene. *Earth and Planetary Science Letters*, *369–370*, 248–259.

Kleiven, H. F., Kissel, C., Laj, C., Ninnemann, U. S., Richter, T. O., & Cortijo, E. (2008). Reduced North Atlantic deep water coeval with the glacial lake Agassiz freshwater outburst. *Science*, *319*(5859), 60–64. https://doi.org/10.1126/science.1148924

Lambelet, M., van de Flierdt, T., Crocket, K., Rehkämper, M., Kreissig, K., Coles, B., et al. (2016). Neodymium isotopic composition and concentration in the western North Atlantic Ocean: results from the GEOTRACES GA02 section. *Geochimica et Cosmochimica Acta*, *177*, 1–29. https://doi.org/10.1016/j.gca.2015.12.019

Lippold, J., Grützner, J., Winter, D., Lahaye, Y., Mangini, A., & Christl, M. (2009). Does sedimentary ^{231}Pa/^{230}Th from the Bermuda Rise monitor past Atlantic Meridional Overturning Circulation? *Geophysical Research Letters*, *36*, L12601. https://doi.org/10.1029/2009GL038068

Lippold, J., Gutjahr, M., Blaser, P., Christner, E., Ferreira, M.-L. C., Mulitza, S., et al. (2016). Deep water provenance and dynamics of the (de)glacial Atlantic meridional overturning circulation. *Earth and Planetary Science Letters*, *445*, 68–78. https://doi.org/10.1016/j.epsl.2016.04.013

Luo, Y., Francois, R., & Allen, S. (2010). Sediment ^{231}Pa/^{230}Th as a recorder of the rate of the Atlantic meridional overturning circulation: insights from a 2-D model. *Ocean Science*, *6*(1), 381–400. https://doi.org/10.5194/os-6-381-2010

Lynch-Stieglitz, J. (2017). The Atlantic Meridional Overturning Circulation and abrupt climate change. *Annual Review of Marine Science*, *9*, 83–104. https://doi.org/10.1146/annurev-marine-010816-060415

Marchal, O., Francois, R., Stocker, T., & Joos, F. (2000). Ocean thermohaline circulation and sedimentary ^{231}Pa/^{230}Th ratio. *Paleoceanography*, *15*(6), 625–641. https://doi.org/10.1029/2000PA000496

Marchitto, T., & Broecker, W. (2006). Deep watermass geometry in the glacial Atlantic ocean: A review of constraints from the paleonutrient proxy Cd/Ca. *Geochemistry, Geophysics, Geosystems*, *7*, Q12003. https://doi.org/10.1029/2006GC001323

Matero, I. S. O., Gregoire, L. J., Ivanovic, R. F., Tindall, J. C., & Haywood, A. M. (2017). The 8.2 ka cooling event caused by Laurentide ice saddle collapse. *Earth and Planetary Science Letters*, *473*, 205–214. https://doi.org/10.1016/j.epsl.2017.06.011

McManus, J., Francois, R., Gherardi, J., Keigwin, L., & Brown-Leger, S. (2004). Collapse and rapid resumption of Atlantic meridional circulation linked to deglacial climate change. *Nature*, *428*(6985), 834–837. https://doi.org/10.1038/nature02494

McManus, J., Oppo, D., & Cullen, J. (1999). A 0.5-million-year record of millennial-scale climate variability in the North Atlantic. *Science*, *283*(5404), 971–975. https://doi.org/10.1126/science.283.5404.971

Mjell, T. L., Ninnemann, U. S., Eldevik, T., & Kleiven, H. K. F. (2015). Holocene multidecadal- to millennial-scale variations in Iceland-Scotland overflow and their relationship to climate. *Paleoceanography*, *30*, 558–569. https://doi.org/10.1002/2014PA002737

Moffa-Sánchez, P., & Hall, I. R. (2017). North Atlantic variability and its links to European climate over the last 3000 years. *Nature Communications*, *8*(1), 1726. https://doi.org/10.1038/s41467-017-01884-8

Moffa-Sanchez, P., Hall, I. R., Thornalley, D. J. R., Barker, S., & Stewart, C. (2015). Changes in the strength of the Nordic Seas Overflows over the past 3000 years. *Quaternary Science Reviews*, *123*, 134–143. https://doi.org/10.1016/j.quascirev.2015.06.007

Morrill, C., LeGrande, A. N., Renssen, H., Bakker, P., & Otto-Bliesner, B. L. (2013). Model sensitivity to North Atlantic freshwater forcing at 8.2 ka. *Climate of the Past*, *9*(2), 955–968. https://doi.org/10.5194/cp-9-955-2013

Müller, R., & Schneider, R. (1993). An automated leaching method for the determination of opal in sediments and particulate matter. *Deep-See Research I*, *40*(3), 425–444. https://doi.org/10.1016/0967-0637(93)90140-X

Ng, H. C., Robinson, L. F., McManus, J. F., Mohamed, K. J., Jacobel, A. W., Ivanovic, R. F., et al. (2018). Coherent deglacial changes in western Atlantic Ocean circulation. *Nature Communications*, *9*, 2947. https://doi.org/10.1038/s41467-018-05312-3

Oppo, D. W., Gebbie, G., Huang, K.-F., Curry, W. B., Marchitto, T. M., & Pietro, K. R. (2018). Data constraints on glacial Atlantic Water wass geometry and properties. *Paleoceanography and Paleoclimatology*, *33*, 1013–1034. https://doi.org/10.1029/2018PA003408

Oppo, D. W., McManus, J. F., & Cullen, J. L. (2003). Deepwater variability in the Holocene epoch. *Nature*, *422*(6929), 277. https://doi.org/10.1038/422277b

Piotrowski, A., Goldstein, S., Hemming, S., & Fairbanks, R. (2005). Temporal relationships of carbon cycling and ocean circulation at glacial boundaries. *Science*, *307*(5717), 1933–1938. https://doi.org/10.1126/science.1104883

Pöppelmeier, F., Blaser, P., Gutjahr, M., Süfke, F., Thornalley, D. J. R., Grützner, J., et al. (2019). Influence of ocean circulation and benthic exchange on deep Northwest Atlantic Nd isotope records during the past 30,000 years. *Geochemistry, Geophysics, Geosystems*, *20*(9), 4457–4469. https://doi.org/10.1029/2019GC008271

Pöppelmeier, F., Gutjahr, M., Blaser, P., Keigwin, L. D., & Lippold, J. (2018). Origin of abyssal NW Atlantic water masses since the Last Glacial Maximum. *Paleoceanography and Paleoclimatology*, *33*, 530–543. https://doi.org/10.1029/2017PA003290

Praetorius, S., McManus, J., Oppo, D., & Curry, W. (2008). Episodic reductions in bottom-water currents since the last ice age. *Nature Geoscience*, *1*(7), 449–452. https://doi.org/10.1038/ngeo227

Rahmstorf, S., Box, J. E., Feulner, G., Mann, M. E., Robinson, A., Rutherford, S., & Schaffernicht, E. J. (2015). Exceptional twentieth-century slowdown in Atlantic Ocean overturning circulation. *Nature Climate Change*, *5*(5), 475–480. https://doi.org/10.1038/nclimate2554

Reimer, P. J., Bard, E., Bayliss, A., Beck, J., Blackwell, P., Bronk Ramsey, C., et al. (2013). IntCal13 and Marine13 radiocarbon age calibration curves 0–50,000 years cal BP. *Radiocarbon*, *55*(4), 1869–1887. https://doi.org/10.2458/azu_js_rc.55.16947

Rempfer, J., Stocker, T. F., Joos, F., Lippold, J., & Jaccard, S. L. (2017). New insights into cycling of ^{231}Pa and ^{230}Th in the Atlantic Ocean. *Earth and Planetary Science Letters*, *468*, 27–37. https://doi.org/10.1016/j.epsl.2017.03.027

Renssen, H., Goosse, H., & Fichefet, T. (2005). Contrasting trends in North Atlantic deep-water formation in the Labrador Sea and Nordic Seas during the Holocene. *Geophysical Research Letters*, *32*, L08711. https://doi.org/10.1029/2005GL022462

Roberts, N., Piotrowski, A., McManus, J., & Keigwin, L. (2010). Synchronous deglacial overturning and water mass source changes. *Science*, *327*(5961), 75–78. https://doi.org/10.1126/science.1178068

Schmittner, A., Gruber, N., Mix, A. C., Key, R. M., Tagliabue, A., & Westberry, T. K. (2013). Biology and air-sea gas exchange controls on the distribution of carbon isotope ratios (δ^{13}C) in the ocean. *Biogeosciences*, *10*(9), 5793–5816. https://doi.org/10.5194/bg-10-5793-2013

Stichel, T., Hartman, A. E., Duggan, B., Goldstein, S. L., Scher, H., & Pahnke, K. (2015). Separating biogeochemical cycling of neodymium from water mass mixing in the Eastern North Atlantic. *Earth and Planetary Science Letters*, *412*, 245–260. https://doi.org/10.1016/j.epsl.2014.12.008

Süfke, F., Lippold, J., & Happel, S. (2018). Improved separation of Pa from Th and U in marine sediments with TK400 Resin. *Analytical Chemistry*, *90*(2), 1395–1401. https://doi.org/10.1021/acs.analchem.7b04723

Tanaka, T., Togashi, S., Kamioka, H., Amakawa, H., Kagami, H., Hamamoto, T., et al. (2000). JNdi-1: A neodymium isotopic reference in consistency with La Jolla neodymium. *Chemical Geology*, *168*(3-4), 279–281. https://doi.org/10.1016/S0009-2541(00)00198-4

Teal, L. R., Bulling, M. T., Parker, E. R., & Solan, M. (2008). Global patterns of bioturbation intensity and mixed depth of marine soft sediments. *Aquatic Biology*, *2*(3), 207–218. https://doi.org/10.3354/ab00052

Thomas, E. R., Wolff, E. W., Mulvaney, R., Steffensen, J. P., Johnsen, S. J., Arrowsmith, C., et al. (2007). The 8.2 ka event from Greenland ice cores. *Quaternary Science Reviews*, *26*(1-2), 70–81. https://doi.org/10.1016/j.quascirev.2006.07.017

Thornalley, D. J. R., Blaschek, M., Davies, F. J., Praetorius, S., Oppo, D. W., McManus, J. F., et al. (2013). Long-term variations in Iceland–Scotland overflow strength during the Holocene. *Climate of the Past*, *9*(5), 2073–2084. https://doi.org/10.5194/cp-9-2073-2013

Thornalley, D. J. R., Oppo, D. W., Ortega, P., Robson, J. I., Brierley, C. M., Davis, R., et al. (2018). Anomalously weak Labrador Sea convection and Atlantic overturning during the past 150 years. *Nature*, *556*(7700), 227–230. https://doi.org/10.1038/s41586-018-0007-4

Voigt, I., Mulitza, S., Chiessi, C. M., Mackensen, A., Lippold, J., Zabel, M., et al. (2017). Variability in the mid-depth ventilation of the western Atlantic Ocean during the last deglaciation. *Paleoceanography*, *32*, 948–965. https://doi.org/10.1002/2017PA003095

Wacker, L., Lippold, J., Molnár, M., & Schulz, H. (2013). Towards single-foraminifera-dating with a gas ion source. *Nuclear Instrument Methods B*, *294*, 307–310. https://doi.org/10.1016/j.nimb.2012.08.038

Yu, E., Francois, R., & Bacon, M. (1996). Similar rates of modern and last-glacial ocean thermohaline circulation inferred from radiochemical data. *Nature*, *379*(6567), 689–694. https://doi.org/10.1038/379689a0